SUPPORTING INFORMATION

Doxorubicin-functionalized silica nanoparticles incorporated into a thermoreversible hydrogel and intraperitoneally administered result in high prostate antitumor activity and reduced cardiotoxicity of doxorubicin

Camila P. Silveira,[†,‡] *Letícia M. Apolinário,*[§] *Wagner J. Fávaro,*[*,§,⊥] *Amauri J. Paula,*[*,#] *Nelson Durán*[†,‡,⊥,¥]

[†]Laboratory of Biological Chemistry, Institute of Chemistry, Universidade Estadual de Campinas (UNICAMP), R. Monteiro Lobato, P.O. BOX 6154, 13083-970, Campinas-SP, Brazil

[‡]NanoBioss, Institute of Chemistry, Universidade Estadual de Campinas (UNICAMP), R. Monteiro Lobato, P.O. BOX 6154, 13083-970, Campinas-SP, Brazil

[§]Department of Structural and Functional Biology, Institute of Biology, Universidade Estadual de Campinas (UNICAMP), R. Monteiro Lobato, P.O. BOX 6109, 13083-865, Campinas-SP, Brazil

[⊥]Farmabrasilis R&D Division, Campinas-SP, Brazil

[#]Solid-Biological Interface Group (SolBIN), Department of Physics, Universidade Federal do Ceará (UFC), Campus do Pici, P.O. BOX 6030, 60440-900, Fortaleza-CE, Brazil

Corresponding Authors

* Tel.: +55 19 3521 6104; email: wjfavaro@gmail.com

* Tel.: +55 85 3366 9270; email: amaurijp@gmail.com

[¥]Current address: Laboratório Nacional de Nanotecnologia (LNNano), Centro Nacional de Pesquisa em Energia e Materiais - CNPEM, Campinas-SP, Brazil

SUMMARY

A. MATERIALS AND METHODS

A1. On the colloidal stabilization by repulsive depletion forces

The stabilization of colloids depends on the balance between repulsive and attractive forces, being unstable when attractive overcome the repulsive.[1] On the course of Brownian motion, nanoparticles often collide and in these collisions they can be so attracted as to aggregate.[2] Thus, they lose mobility and the more aggregation occurs, the heavier and less mobile they turn until they reach such a size that phase separation occurs.[2] For a colloid to be stable, there must be something that hampers or decreases the attraction between particles, for example, electrostatic or steric stabilization.[1,2] The first ensures that there is repulsion between the particles by electric charges of the same sign through the manifestation of coulombic forces. The second involves the use of polymeric materials (or long chain materials) adsorbed onto the particle surface, so that the approach of the chains results in an increase in the free energy of the system, causing sufficient repulsion to stabilize the colloid. The magnitude of the free energy variation depends on the characteristics of the chain-chain interactions as well as the chain-medium interactions. Considering an aqueous dispersion and a liophilic polymer, for instance, an increase in the chain-chain interactions causes an increase in the free energy, resulting in repulsion.[1,2] On the other hand, if the dispersing medium is a solvent with low interactivity, the chain-chain interactions are favored, resulting in attraction.[1] Since $\Delta G = \Delta H - T\Delta S$, the increase in the free energy (ΔG) resulting from the chain-chain interaction can be manifested through an increase in enthalpy (ΔH) and/or a decrease in entropy (ΔS).[1] The first involves the breaking of bonds between the polymer and the solvent as the chain-chain interactions increase, being independent of the temperature. The second involves the loss of conformational degrees of freedom as the chain-chain interactions

increase, being dependent of the temperature.[1] However, these considerations depict homogeneous systems in which the polymeric chain is firmly adsorbed on the particle surface, disregarding possible sorption equilibrium, micelle formation[2] or fluctuations in the distribution density of the polymeric chains throughout the volume. Considering a bit more complex suspension, composed of two particle species – large particles and small particles, the attraction or repulsion of the big particles is related to the entropic forces originated from the osmotic pressure and from the excluded volume effect.[3] These forces are called depletion forces and they were firstly studied by Asakura and Oosawa, who developed a model that describes the depletion force for low concentrations of small particles.[4] Their model considers large particles with diameters of $D=2R_b$ in a solution of small particles with diameters of $d=2R_s$ (Figure S1a). Around each particle there is a volume, called depletion zone, in which the centers of the small particles cannot penetrate (excluded volume effect). When two large particles approach each other in such a way that their depletion zones overlap (i.e. the excluded volume is reduced) and no small particle can occupy the space between the large particles, the difference between the local osmotic pressure and the bulk osmotic pressure results in an attractive force (Figure S1b).

This force is purely entropic, as a decrease in the excluded volume increases the available volume for the small particles. According to Asakura-Oosawa,[3] the depletion force Fd (Eq. 1) is null when the distance between two large particles is greater than or equal to the small particle diameter, and non-zero when this distance is smaller than the small particle diameter:

$$F_d = \begin{cases} 0, & h \geq d + D \\ -p_0 S, & h < d + D \end{cases} \qquad \textbf{Equation 1}$$

Where h is the distance between the large particles, $p_0 = \rho k_B T$ (where ρ is the density number of the small particles) and S is the circular area associated to the overlapping volume. The Asakura-Oosawa model[3] considers that the local density of small particles only changes when h < d + D. However, the local density of small particles varies due to the potential generated by two large particles, even for h = d + D. Therefore, the limitation of Asakura-Oosawa model to explain the depletion force lies in the fact that F_d will always be attractive (represented by the negative sign in Eq. 1). It is therefore sufficient to describe suspensions with low small particle concentrations, where the interactive potential between small particles is neglected. So, to overcome this limitation, one must use a theory derived from the perturbation theory of liquids,[4] which considers all the interactions occurring between all particles. At high concentrations of small particles, the correlation between them are so significant that they can interfere in the interactions so as to include a repulsive component.[5] In such cases, a correlation function g(r) needs to be included, which is related to the depletion potential V(r) (Eq. 2), where r is the distance from the center of the large particle along the axis. This correlation function g(r) is then a factor that multiplies the bulk density ρ to provide a local density ρ(r) for a given particle (Eq. 3).

$$V(r) = -k_B T \ln g(r) \qquad \textbf{Equation 2}$$

$$\rho(r) = \rho g(r) \qquad \textbf{Equation 3}$$

To solve g(r) and then obtain an equation to the depletion potential that would consider a negative component, theories such as Ornstein-Zernike and Pervus-Yevick were used.[4] Ornstein-Zernike considers that g(r) depends on the direct correlation between particles and on all the indirect correlations in the system.[4] In summary,

therefore, it can be said that the depletion potential is closely related to the correlation between all particles that, in turn, is related to the local density. Theoretical simulations and experimental results of the depletion force show an oscillatory curve, with peaks (repulsion) and valleys (attraction) as a function of the large particles separation, as shown in Crocker et al. (1999) work.[5] The authors show that at higher concentrations of small particles, the interactive potential curve starts to have an oscillatory profile, qualitatively associated to the layers of small particles. Once the interactive potential between large particles depend on their separation, when the separation is a multiple integer of the diameter of the small particles ($2R_s$), i.e. the separation between large particles correspond to an integer number of layers, the interactive potential is repulsive (Figure S1c). When the separation between large particles is not sufficient to accommodate an integer number of small particles, the interactive potential is attractive (Figure S1d). The scientific community believes that at high concentrations of small particles, these form layers around the large particles, hampering the attraction between them and originating the repulsion peaks.[5] It is therefore possible to correlate the repulsive depletion force with the correlation length ξ (length scale that correlates two particles) of the small particles: the repulsion starts to appear when the large particles separation is greater than ξ.[6]

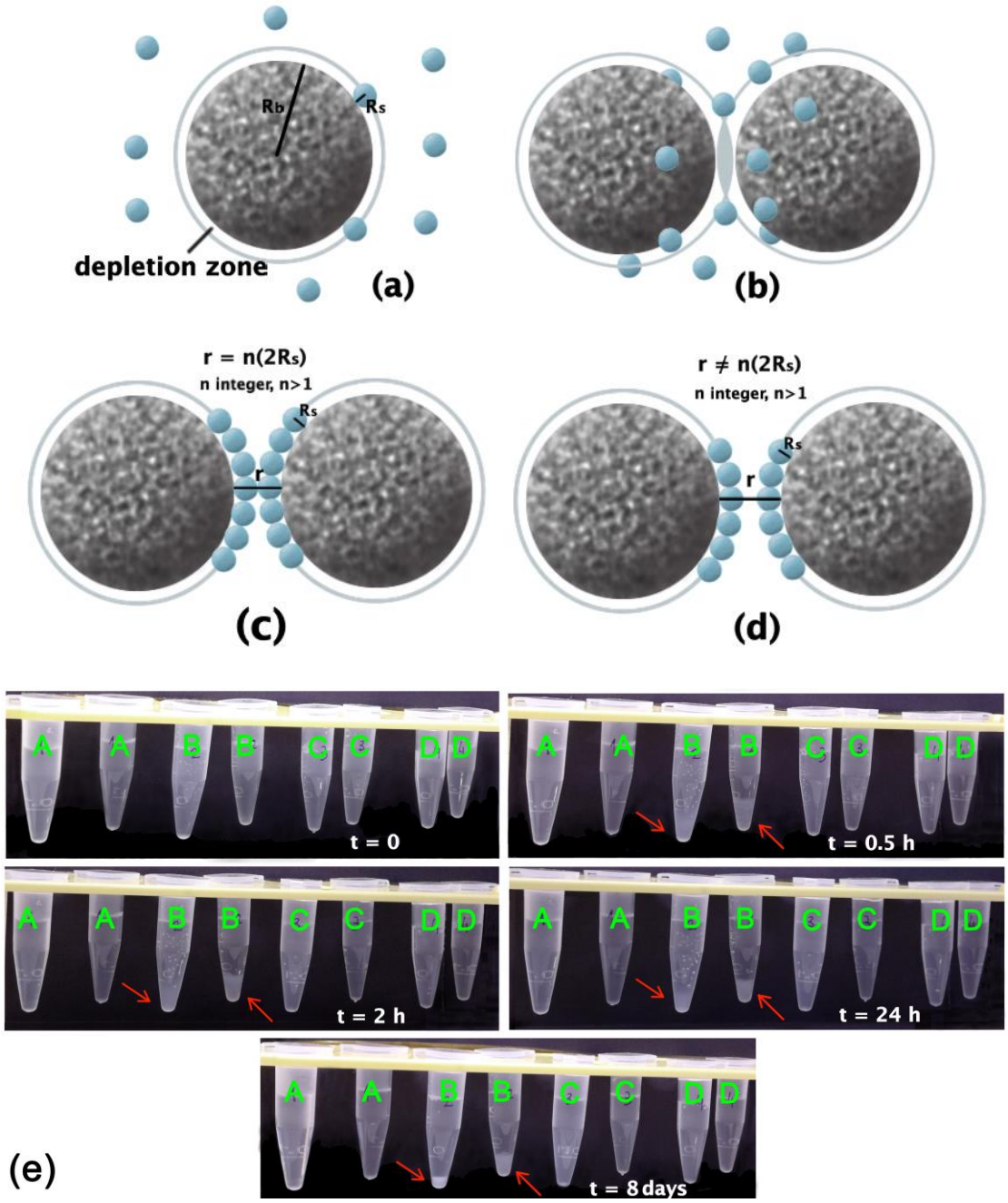

Figure S1. Illustration of the (a) depletion zone (or excluded volume), which thickness is R_s; (b) overlap of the depletion zones of two large particles, resulting in a reduction of the excluded volume; (c) repulsive and (d) attractive interactive potential of large particles as a function of their separation. (e) Photographs of MSNs (500 µg mL^{-1}) colloidal suspensions in NaCl 0.9% in various PF127 concentrations (A= 0%; B= 0.1%; C= 1.0%; D= 5.0%) along 8 days.

A2. Colloidal stability of MSNs: quantification through ICP-OES

The MSNs quantification on the colloidal stability assays was accomplished through ICP-OES. This spectrophotometric technique allows quantifying chemical elements through the emitted light intensity in specific wavelengths that are related to each element in the periodic table.[7] The sample is atomized and ionized by plasma at high temperature (~6000 K), which causes not only the atoms dissociation but also a great amount of collisional excitation and ionization.[7] Since the atoms and ions are in the excited state, they can decay to lower energy states and emit light in specific wavelengths, which is measured and used to determine the concentration of the elements of interest.[7] Once the sample is composed by silica nanoparticles, which are very stable in neutral pH,[8,9] it is necessary to ensure that the degradation of the particles into monomeric species of silicon is complete. Therefore, before the conducting the analyses, the nanoparticles left in the supernatant were degraded in pH 11.6 by the addition of KOH solution (pH 12.0, 0.01 mol L^{-1}). Keeping the pH higher than 11.0 ensures the silica dissolution (into $HSiO^{3-}$ or SiO^{3-}), while pHs between 4.0 and 10.8 are suitable for particle growth and aggregation.[8] To avoid damaging the equipment, the pH was neutralized (pH 7.0) with HCl (pH 2.0, 0.01 mol L^{-1}) instants before each measurement, avoiding nucleation and particle growth in neutral pH.

A3. Synthesis and characterization of hydrogel-hybrid systems

DOX concentration in hybrid systems (1.25 mg mL^{-1}) was calculated to reach 1.5 mg kg^{-1} considering a 300 µL application and an average rat weight of 150 g. To accomplish the dissolution and release assay, the release medium was put carefully on the hydrogel surface as illustrated in Figure S2.

Figure S2. Illustration of the membraneless hydrogel dissolution method.

A4. *In vivo* assay: prostate cancer induction

Seventeen Fischer 344 rats (male, 7-week-old) were used in the *in vivo* study, while prostate cancer induction was performed in 13, following a new protocol developed by Fávaro et al.[20] The new protocol uses a formulation for controlled release of the carcinogenic agent *N*-methyl-*N*-nitrosourea (MNU), which ensures the appearance of prostate cancer in 100% of the animals as well as the presence of pre-malign lesions, making the model suitable to study prostatic carcinogenesis since these lesions are also present in human clinical status. The induction procedure consisted firstly by a daily subcutaneous injection of 100 mg kg^{-1} testosterone cypionate diluted in 0.5 mL of peanut oil for three days. Then, the animals were anesthetized with 2% xylazine hydrochloride (5 mg kg^{-1}) and 10% ketamyne hydrochloride (60 mg kg^{-1}) for further perform of 0.5 cm suprapubic incision and inoculation of 0.2 mL of 15 mg kg^{-1} MNU dissolved in 0.3 mL of sodium citrate (1 M, pH 6.0) and PF127 25%, which allows *in situ* gelation of the solution. After one week from the MNU inoculation, the animals received subcutaneous injections of 5 mg kg^{-1} testosterone cypionate diluted in 5 mL of peanut oil on alternate days for 120 days.

B. RESULTS

B1. UV-Vis light absorption characterization of the components studied

To ensure that DOX quantification could be accomplished through UV-Vis light absorption, the system components were characterized through this technique. From the results (Figure S3), it can be seen that DOX spectra presents an absorption peak at 480 nm (chosen for the quantification) that does not overlap with MSNs, PF127 or BSA (used in DOX release assay) spectra.

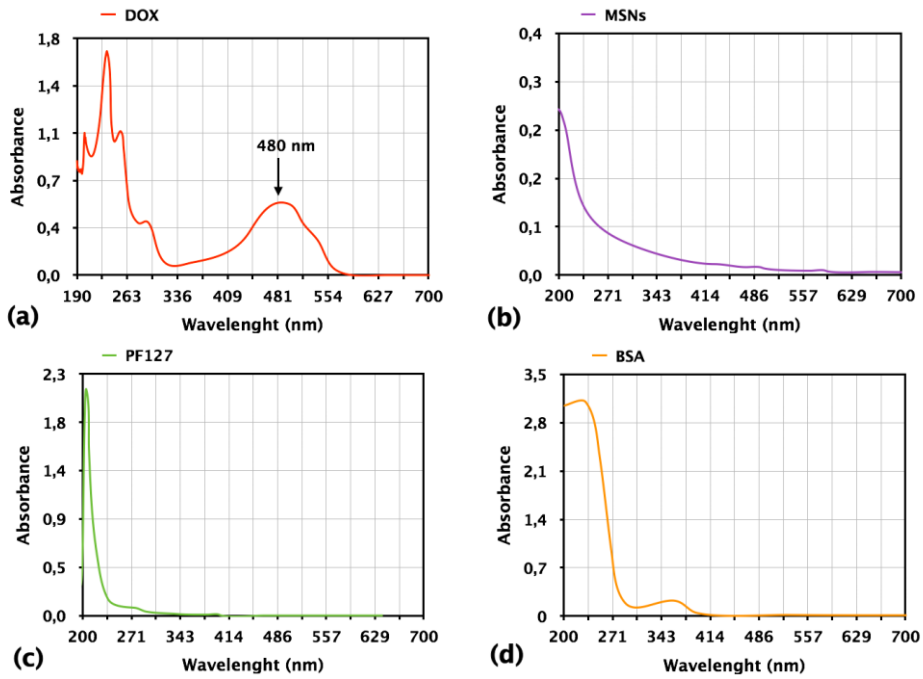

Figure S3. UV-Vis light absorption spectra of **(a)** DOX (125 µg mL^{-1}), with the arrow indicating the peak at 480 nm, **(b)** MSNs (150 µg mL^{-1}), **(c)** PF127 5% (w/w) and **(d)** BSA (500 µg mL^{-1}).

B2. MSNs characterization: adsorption isotherms

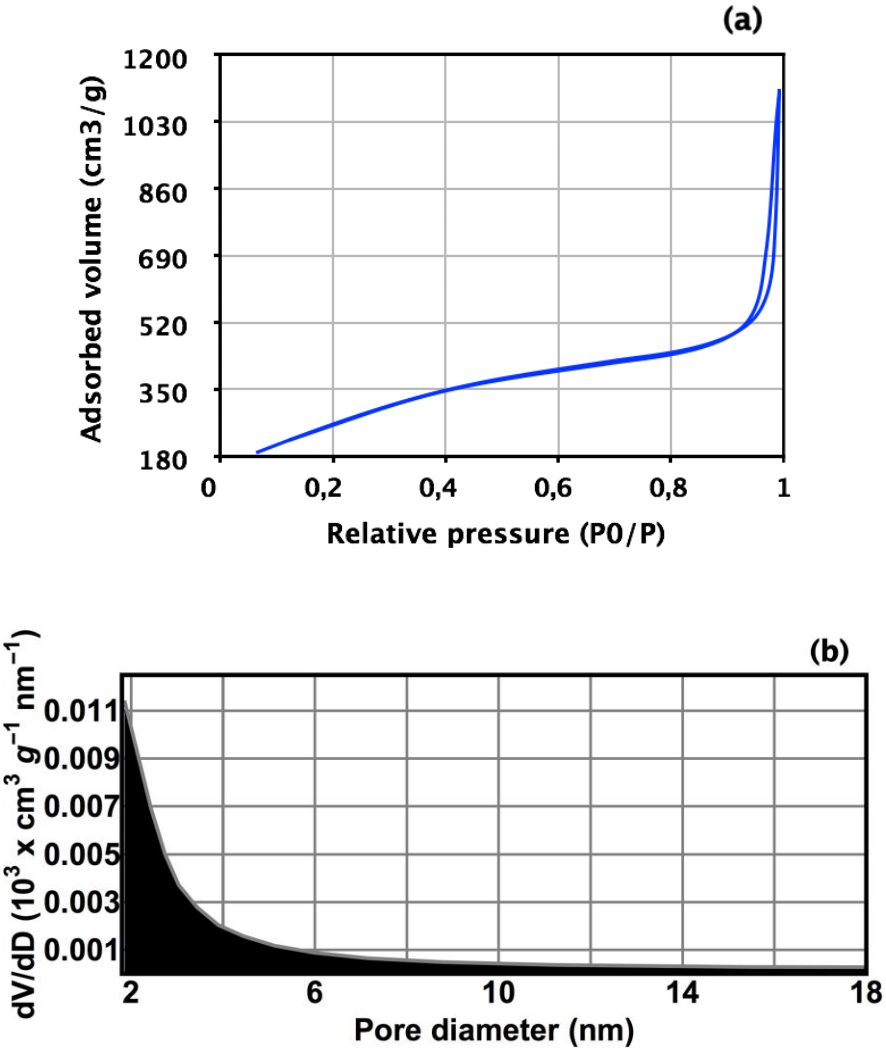

Figure S4. (a) Pore size distribution of MSNs indicating pores around 2 nm, **(b)** nitrogen sorption isotherm for MSNs.

B3. ζ-potential of MSNs with increasing PF127 concentrations

To confirm that the PF127 was adsorbing on the surface of the nanoparticles, a ζ-potential assay was performed for MSN-samples with increasing PF127 concentrations. In the case of the MSNs colloidal suspension in water (ζ around –20.0 mV), the stabilization occurs electrostatically by the repulsion of the negatively charged MSNs with deprotonated silanol surface groups. Based on the aggregation assay as a function of time, the ζ-potential assay was performed for samples with

PF127 concentrations from 0.1% to 1.0% (Figure S5). With the addition of 0.1wt% of PF127 (neutral polymer), the ζ-potential becomes considerably less negative (close to neutrality), indicating the interaction of PF127 on the nanoparticle surface. It is possible that PF127 is adsorbed on the surface of MSNs, but also that there is a micellar layer surrounding them (or both). In this case, to explain the MSNs colloidal stability it must be considered steric effects as well as depletion forces, i.e. the interactions of the MSNs with PF127 occurs in long and short ranges.

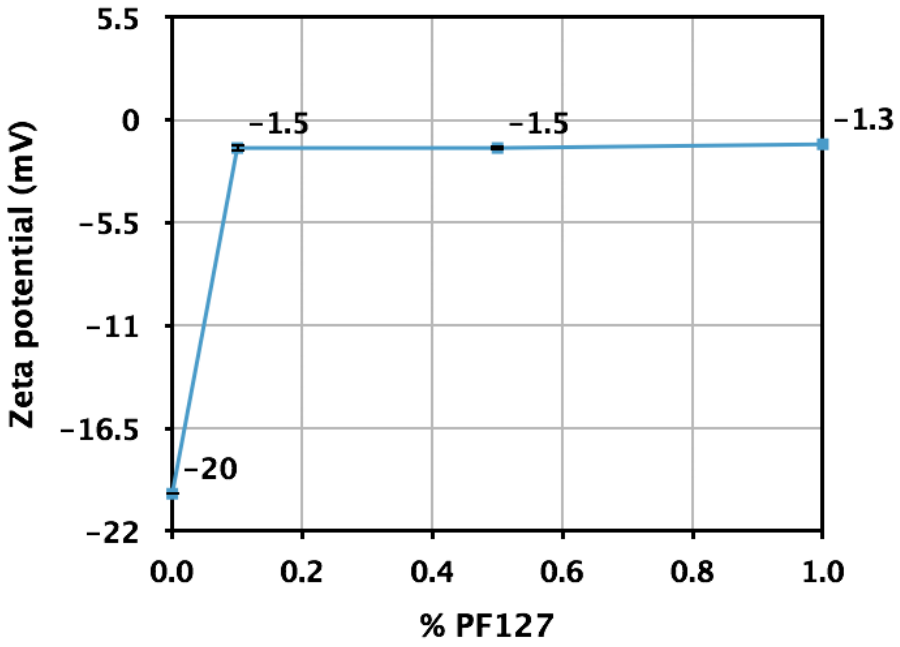

Figure S5. ζ-potential of the MSNs (250 µg mL^{-1}) as a function of the PF127 concentration in 10x diluted PBS solution.

B4. Gelation temperature assay

To determine the PF127 concentration to be used in the hybrid systems to ensure the hydrogel formation, we first considered the gelation temperature (T_{gel}) of PF127 solutions in different compositions. The systems would be administered via intraperitoneal in rats (Fischer 344), which body temperature is 35°C. Therefore, the T_{gel} range considered acceptable for this purpose would be around 20°C, which ensures an easier manipulation of the liquid formulation, preventing gelation inside syringe needles. Likewise, a T_{gel} too close to the rats' body temperature could retard the hydrogel formation inside the animals, making the system to leak to other locations.

At first, the T_{gel} assays were performed for PF127 in physiological saline solutions (Table S1) and then DOX and MSNs were included (Table S2). From the results illustrated in Table S1, PF127 concentrations lower than 15% were excluded, since the T_{gel} exceeded 30°C, which could hinder or delay the gelation of the systems after the administration. Similarly, PF127 concentrations above 28% were also excluded since T_{gel} were too low and could im the manipulation of the solutions during the administration. After completing the T_{gel} assays for the systems containing MSNs and DOX, it was concluded that the PF127 composition that would better fit to *in vivo* assay was of 18%.

Table S1. T_{gel} for PF127 in physiological saline solutions.

%PF127	T_{gel} (°C)	%PF127	T_{gel} (°C)
30	9.5 ± 0.5	22	16.5 ± 0.5
28	11.0 ± 0.5	18	21.0 ± 0.5
25	14.0 ± 0.5	15	> 30.0 ± 0.5

Table S2. T_{gel} for PF-127 solutions containing MSNs and DOX.

Condition	%PF127	T_{gel} (°C)	Condition	%PF127	T_{gel} (°C)
Absence of MSNs	25	14.0 ± 0.5	**MSNs (1 mg mL^{-1})**	25	14.0 ± 0.5
	22	17.0 ± 0.5		22	17.0 ± 0.5
	18	21.0 ± 0.5		18	21.0 ± 0.5

* DOX concentration in all samples was 1.25 mg mL^{-1}

C. REFERENCES

(1) Shaw, D. *Introduction to Colloid & Surface Chemistry*; 4th ed.; Butterworth-Heinemann: Eastbourne, 1992.

(2) Hunter, R. J. *Introduction to Modern Colloid Science*; 1st ed.; Oxford University Press: Oxford, 1993.

(3) Asakura, S.; Oosawa, F. Interaction between Particles Suspended in Solutions of Macromolecules. *J. Polym. Sci.* **1958**, *33*, 183–192.

(4) McQuarrie, D. *Statistical Mechanics*; Harper & Row: New York, 1976.

(5) Crocker, J.; Matteo, J.; Dinsmore, a.; Yodh, a. Entropic Attraction and Repulsion in Binary Colloids Probed with a Line Optical Tweezer. *Phys. Rev. Lett.* **1999**, *82*, 4352–4355.

(6) Zhang, X.; Servos, M. R.; Liu, J. Ultrahigh Nanoparticle Stability against Salt, pH, and Solvent with Retained Surface Accessibility via Depletion Stabilization. *J. Am. Chem. Soc.* **2012**, *134*, 9910–9913.

(7) Boss, C. B.; Freeden, K. J. *Concepts, Instrumentation and Techniques in Inductively Coupled Plasma Optical Emission Spectrometry*; 3rd ed.; Shelton, 2004.

(8) Brinker, C. J.; Scherer, G. W. *Sol-Gel Science : The Physics and Chemistry of Sol-Gel Processing*; Academic Press: Boston, 1990.

(9) Paula, A. J.; Montoro, L. a; Filho, A. G. S.; Alves, O. L. Towards Long-Term Colloidal Stability of Silica-Based Nanocarriers for Hydrophobic Molecules: Beyond the Stöber Method. *Chem. Commun.* **2012**, *48*, 591–593.

(10) Cedervall, T.; Lynch, I.; Lindman, S.; Berggård, T.; Thulin, E.; Nilsson, H.; Dawson, K. A.; Linse, S. Understanding the Nanoparticle-Protein Corona Using Methods to Quantify Exchange Rates and Affinities of Proteins for Nanoparticles. *Proc. Natl. Acad. Sci. U. S. A.* **2007**, *104*, 2050–2055.

(11) Monopoli, M. P.; Walczyk, D.; Campbell, A.; Elia, G.; Lynch, I.; Bombelli, F. B.; Dawson, K. A. Physical-Chemical Aspects of Protein Corona: Relevance to in Vitro and in Vivo Biological Impacts of Nanoparticles. *J. Am. Chem. Soc.* **2011**, *133*, 2525–2534.

(12) Nel, A.; Xia, T.; Mädler, L.; Li, N. Toxic Potential of Materials at the Nanolevel. *Science* **2006**, *311*, 622–627.

(13) Gebauer, J. S.; Malissek, M.; Simon, S.; Knauer, S. K.; Maskos, M.; Stauber, R.

H.; Peukert, W.; Treuel, L. Impact of the Nanoparticle−protein Corona on Colloidal Stability and Protein Structure. *Langmuir* **2012**, *28*, 9673–9679.
(14) Monopoli, M. P.; Bombelli, F. B.; Dawson, K. A. Nanobiotechnology: Nanoparticle Coronas Take Shape. *Nat. Nanotechnol.* **2011**, *6*, 11–12.
(15) Monopoli, M. P.; Aberg, C.; Salvati, A.; Dawson, K. A. Biomolecular Coronas Provide the Biological Identity of Nanosized Materials. *Nat. Nanotechnol.* **2012**, *7*, 779–786.
(16) Lundqvist, M.; Stigler, J.; Cedervall, T.; Berggard, T.; Flanagan, M. B.; Lynch, I.; Elia, G.; Dawson, K. A. The Evolution of the Protein Corona around Nanoparticles: A Test Study. **2011**, *5*, 7503–7509.
(17) Dawson, K. A.; Lesniak, A.; Fenaroli, F.; Monopoli, M. P.; Christoffer, A.; Salvati, A. ARTICLE E Ff Ects of the Presence or Absence of a Protein Corona on Silica Nanoparticle Uptake and Impact on Cells. **2012**, 5845–5857.
(18) Paula, A. J.; Araujo Júnior, R. T.; Martinez, D. S. T.; Paredes-Gamero, E. J.; Nader, H. B.; Durán, N.; Justo, G. Z.; Alves, O. L. Influence of Protein Corona on the Transport of Molecules into Cells by Mesoporous Silica Nanoparticles. *ACS Appl. Mater. Interfaces* **2013**, *5*, 8387–8393.
(19) Salvati, A.; Pitek, A. S.; Monopoli, M. P.; Prapainop, K.; Bombelli, F. B.; Hristov, D. R.; Kelly, P. M.; Åberg, C.; Mahon, E.; Dawson, K. A. Transferrin-Functionalized Nanoparticles Lose Their Targeting Capabilities When a Biomolecule Corona Adsorbs on the Surface. *Nat. Nanotechnol.* **2013**, *8*, 137–143.
(20) Fávaro, W. J.; Apolinário, L. M.; Caballero, N.; Garcia, P. V; Bueno, C. P. S. Composição Para Liberação Controlada de Carcinógeno E Uso. Patent BR 10 2014 023118 8, 2014.